arXiv:1609.01021v1 [cond-mat.supr-con] 5 Sep 2016

Spin excitations in optimally P-doped $BaFe_2(As_{0.7}P_{0.3})_2$ superconductor

Ding Hu,[1,2] Zhiping Yin,[1,3,*] Wenliang Zhang,[2] R. A. Ewings,[4] Kazuhiko Ikeuchi,[5] Mitsutaka Nakamura,[6] Bertrand Roessli,[7] Yuan Wei,[2] Lingxiao Zhao,[2] Genfu Chen,[2] Shiliang Li,[2,8] Huiqian Luo,[2] Kristjan Haule,[3] Gabriel Kotliar,[3,9] and Pengcheng Dai[10,1,†]

[1]*Center for Advanced Quantum Studies and Department of Physics, Beijing Normal University, Beijing 100875, China*
[2]*Beijing National Laboratory for Condensed Matter Physics, Institute of Physics, Chinese Academy of Sciences, Beijing 100190, China*
[3]*Department of Physics, Rutgers University, Piscataway, NJ 08854, USA*
[4]*ISIS Facility, STFC Rutherford Appleton Laboratory, Harwell Oxford, Didcot, OX11 0QX, United Kingdom*
[5]*Research Center for Neutron Science and Technology, Comprehensive Research Organization for Science and Society (CROSS), Tokai, Ibaraki 319-1106, Japan*
[6]*Materials and Life Science Division, J-PARC Center, Tokai, Ibaraki 319-1195, Japan*
[7]*Laboratory for Neutron Scattering and Imaging, Paul Scherrer Institut, CH-5232 Villigen, Switzerland*
[8]*Collaborative Innovation Center of Quantum Matter, Beijing, China*
[9]*Brookhaven National Laboratory, Upton, NY 11973-5000, USA*
[10]*Department of Physics and Astronomy, Rice University, Houston, Texas 77005, USA*

We use inelastic neutron scattering to study temperature and energy dependence of spin excitations in optimally P-doped $BaFe_2(As_{0.7}P_{0.3})_2$ superconductor ($T_c = 30$ K) throughout the Brillouin zone. In the undoped state, spin waves and paramagnetic spin excitations of $BaFe_2As_2$ stem from antiferromagnetic (AF) ordering wave vector $\mathbf{Q}_{AF} = (\pm 1, 0)$ and peaks near zone boundary at $(\pm 1, \pm 1)$ around 180 meV. Replacing 30% As by smaller P to induce superconductivity, low-energy spin excitations of $BaFe_2(As_{0.7}P_{0.3})_2$ form a resonance in the superconducting state and high-energy spin excitations now peaks around 220 meV near $(\pm 1, \pm 1)$. These results are consistent with calculations from a combined density functional theory and dynamical mean field theory, and suggest that the decreased average pnictogen height in $BaFe_2(As_{0.7}P_{0.3})_2$ reduces the strength of electron correlations and increases the effective bandwidth of magnetic excitations.

PACS numbers: 75.30.Ds, 25.40.Fq, 75.50.Ee

Since the discovery of unconventional superconductivity in iron pnictides near antiferromagnetic (AF) instability [1–7], a central issue has been whether these materials are fundamentally different from copper oxide superconductors, where the magnetism and superconductivity are derived from Mott physics and its associated electron correlations [8–14]. Since iron pnictides have tetrahedrally coordinated nearest pnictogen atoms, the $3d$ level in Fe ions splits into an e_g state and a few hundred meV higher t_{2g} state [15–22]. Without Hund's rule interaction, the e_g state would be fully occupied with four of the six Fe $3d$ electrons while the remaining two $3d$ electrons should reside in the t_{2g} state crossing the Fermi level. The presence of a strong Hund's coupling J_H, which tends to align spins of all the electrons on a given Fe-atom, competes with the crystal field splitting and promotes high spin states of the Fe $3d$ electrons, resulting in large charge and spin fluctuations. Although it is generally accepted that electron correlations are also present in iron pnictides [11–14], it remains unclear if the correlation strength is controlled by the on-site Hubbard U interaction as in the case of cuprates [8] or arises primarily from the Hund's coupling J_H within one atomic site [15–17]. The local moments formed by the Fe $3d$ electrons, especially those in the d_{xz}, d_{yz}, and d_{xy} orbitals, are coupled to their nearest neighbors by both the direct exchange associated with nearest neighbor Fe-Fe distance and anisotropic superexchange interactions via hopping through the As pnictogen [Figs. 1(a), 1(b), and 1(c)]. By increasing the Fe-pnictogen distance, electron hopping between the nearest Fe ions becomes difficult, and the system is localized with enhanced electron correlations. On the other hand, reducing the Fe-pnictogen distance facilitates the electron hopping, and thus reducing the electron correlations.

Using density functional theory (DFT) combined with dynamical mean field theory (DMFT) suitable for describing the Hund's coupling in iron pnictides [15–17, 23, 24], the evolution of spin excitations in electron and hole-doped $BaFe_2As_2$ can be calculated [25–27]. In particular, the theory predicts that spin-wave and spin excitation bandwidths, defined as the peak in energy dependence of the dynamic susceptibility $\chi''(E)$ integrated near the AF zone boundary $(\pm 1, \pm 1)$ [25, 27], in different iron pnictides are controlled by the iron-pnictogen distance and the valence of the Fe atoms similar to electron correlations [28]. Experimentally, spin-waves and spin excitations in electron and hole-doped AFe_2As_2 (A=Ba, Sr, Ca) family of iron pnictides mapped out by inelastic neutron scattering experiments throughout the Bril-

louin zone [29–33] are qualitatively consistent with the DFT+DMFT calculations and peak around 180 meV near $(1, 1)$ [25, 27]. Although neutron scattering experiments on spin waves of NaFeAs, which has larger pnictogen height ($h_{Pn} = 1.416$ Å) [34] compared with that of $BaFe_2As_2$ [Fig. 1(b), $h_{Pn} = 1.36$ Å], confirm the notion that increasing pnictogen height in iron pnictides decreases the spin-wave bandwidths to ∼110 meV near $(1, 1)$ and increases the electron correlation [35], the crystal structures of NaFeAs and $BaFe_2As_2$ are rather different, and it is still unclear that varying the iron-pnictogen distance within one family of iron pnictides can indeed control the electron correlations and spin excitation spectra.

In this paper, we present inelastic neutron scattering studies of temperature and energy dependence of spin excitations in $BaFe_2(As_{0.7}P_{0.3})_2$ superconductor ($T_c = 30$ K) [3, 6]. We chose $BaFe_2(As_{0.7}P_{0.3})_2$ because it is the optimal isovalently doped $BaFe_2As_2$. At the same time, it has the average pnictogen height ($h_{Pn} = 1.28$ Å) significantly smaller than that of $BaFe_2As_2$ due to the smaller size of the P dopants [Figs. 1(b) and 1(c)] [4]. Since the average pnictogen height of $BaFe_2(As_{1-x}P_x)_2$ decreases continuously from $BaFe_2As_2$ to $BaFe_2(As_{0.7}P_{0.3})_2$ without modifying much the in-plane Fe-Fe distance or changing the valence of Fe [4], we expect weaker electron correlations and wider spin excitation bandwidth in $BaFe_2(As_{0.7}P_{0.3})_2$ compared with that of $BaFe_2As_2$ [28].

Figures 1(d) and 1(e) show the energy dependence of $S(Q, E)$ of spin excitations for $BaFe_2As_2$ and $BaFe_2(As_{0.7}P_{0.3})_2$, respectively. While spin-wave dispersions of $BaFe_2As_2$ reach zone boundary positions $(1, \pm 1)$ around 200 meV [Fig. 1(d)], dispersions of spin excitations of $BaFe_2(As_{0.7}P_{0.3})_2$ become steeper, and reach $(1, \pm 1)$ at energies well above 200 meV [Fig. 1(e)]. Indeed, we find that spin excitations in $BaFe_2(As_{0.7}P_{0.3})_2$ have lower intensity but larger energy bandwidth than that of $BaFe_2As_2$ [30], as revealed in the energy dependence of the dynamic susceptibility $\chi''(E)$ integrated over the dashed vertical lines in Figs. 1(d) and 1(e) ($0.6 \leq H \leq 1.4$ and $0.6 \leq K \leq 1.4$) near the zone boundary $(1, \pm 1)$ [Figs. 1(f) and 1(g)]. These results are also consistent with the energy dependence of the local dynamic susceptibility and DFT+DMFT calculations of $S(Q, E)$ [Fig. 1(h), Figs. 2-4]. Therefore, the decreased average pnictogen height in $BaFe_2(As_{1-x}P_x)_2$ decreases the electron correlations and increases the overall spin excitation energy bandwidths.

Our neutron scattering experiments were carried out on the MAPS and 4SEASONS chopper spectrometers at ISIS, Rutherford Appleton Laboratory, UK and Japan Proton Accelerator Research Complex, Japan, respectively. Some measurements are also carried out on EIGER triple-axis spectrometer in Paul Scherrer Institut, Switzerland. Our $BaFe_2(As_{0.7}P_{0.3})_2$ single crystals were grown by a self-flux method [36]. For P-doped

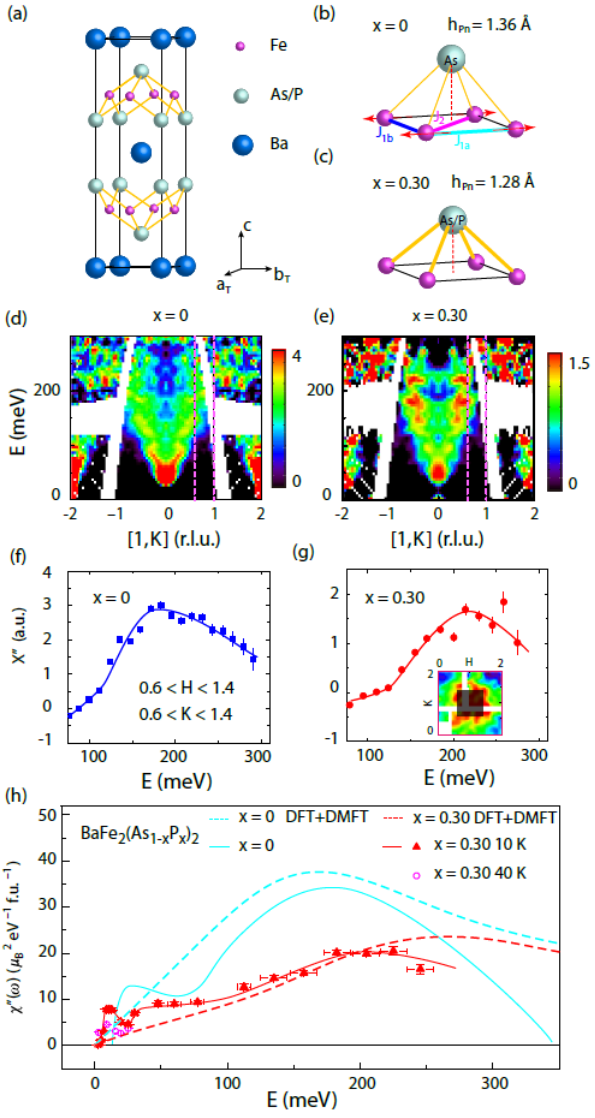

FIG. 1: (a) The crystal structure of $BaFe_2(As_{1-x}P_x)_2$. The purple, silvery and blue balls indicate Fe, As/P, and Ba positions, respectively. (b,c) Schematic diagrams of the FeAs tetrahedron, showing the average iron pnictogen height decreased from 1.36 Å for $BaFe_2As_2$ to 1.28 Å for $BaFe_2(As_{0.7}P_{0.3})_2$ [37]. (d) The energy dependence of $S(Q, E)$ of spin waves of $BaFe_2As_2$ along the $(1, K)$ direction (with integration of H from 0.9 to 1.1 rlu) after subtracting the background integrated from $1.8 < H < 2.2$ and from $-0.25 < K < 0.25$ rlu with $E_i = 450$ meV at $T = 10$ K measured on MAPS [30]. (e) Identical projection for spin excitations of $BaFe_2(As_{0.7}P_{0.3})_2$ obtained on MAPS with $E_i = 450$ meV. The negative scattering below ∼50 meV is due to errors in background subtraction. Energy dependence of wave vector integrated [integration range is shown in the shaded box in the inset of (g)] dynamic susceptibility $\chi''(E)$ for (f) $BaFe_2As_2$ and (g) $BaFe_2(As_{0.7}P_{0.3})_2$. The vertical dashed lines in (d) and (e) show wave vector integration range along the [0,K] direction. (h) Energy dependence of the local dynamic spin susceptibility $\chi''(E)$ for $BaFe_2As_2$ (solid cyan line), $BaFe_2(As_{0.7}P_{0.3})_2$ below (solid red triangle and solid red line) and above (open purple circles) T_c with corrected magnetic form factor. Dashed cyan and red lines are DFT+DMFT calculations for $BaFe_2As_2$ and $BaFe_2(As_{0.7}P_{0.3})_2$, respectively.

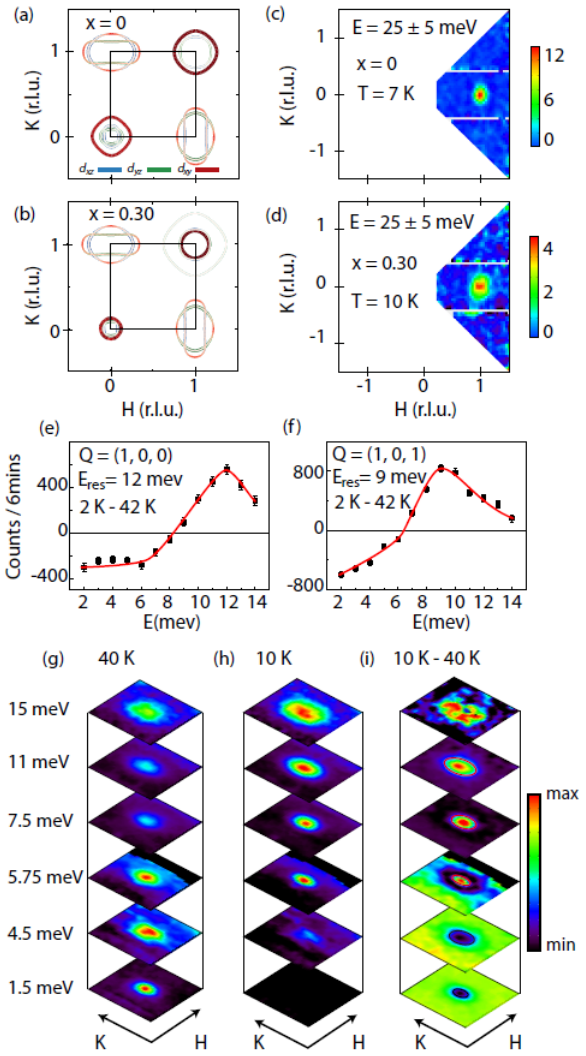

FIG. 2: (a,b) Calculated Fermi surfaces of the d_{xz}, d_{yz}, and d_{xy} orbitals for BFe_2As_2 and $BaFe_2(As_{0.7}P_{0.3})_2$, respectively. (c,d) The corresponding wave vector dependence of the low-energy (E = 25 meV) spin excitations. The color bars represent the vanadium-normalized absolute spin wave intensity in units of mbar/sr/meV/Fe. The temperature differences of constant-wave vector scans at (e) $\mathbf{Q} = (1, 0, 0)$ and (f) $(1, 0, 1)$ blow (2 K) and above (42 K) T_c obtained using the EIGER triple-axis spectrometer. The modulation of resonance (superconductivity-induced intensity gain) with L is consistent with previous experiment [40]. Constant energy slices of the spin excitations as a function of increasing energy (g) at 40 K and (h) 10 K. (i) Temperature difference between 10 K and 40 K, showing clearly intensity gain in the energy region of 8 meV to 11 meV.

$BaFe_2(As_{1-x}P_x)_2$ near $x = 0.3$, the collinear static AF order in $BaFe_2As_2$ is suppressed and superconductivity reaches optimal value at $T_c = 30$ K [37]. We coaligned ∼17 g of single crystals in the $[H, H, L]$ scattering plane with a mosaic <7°. To facilitate easy comparison with spin waves in $BaFe_2As_2$, which has an orthorhombic AF ground state [30], we define the wave vector $\mathbf{Q}$ at (q_x,q_y,q_z) in Å^{-1} as $(H,K,L) = (q_xa/2\pi,q_yb/2\pi,q_zc/2\pi)$ where $a = b \approx 5.6$ Å and $c = 12.87$ Å using the orthorhombic magnetic unit cell notation where low-energy spin excitations are expected to stem from the in-plane wave vector positions $\mathbf{Q}_{AF} = (\pm1, 0)$ and $(0, \pm1)$. For chopper spectrometer inelastic neutron scattering measurements, the incident beam energies were E_i = 35, 80, 250, 450 meV at MAPS and E_i = 13, 21, 82, 313 meV at 4SEASONS with k_i parallel to the c-axis. Spin excitation intensity was normalized to absolute units using a vanadium standard (∼ 30% error).

Since there is no evidence that the P dopant forms long range order in $BaFe_2(As_{1-x}P_x)_2$, we use an effective pnictide position in the DFT+DMFT calculations to simulate the physical consequence of P doping. In $BaFe_2(As_{0.71}P_{0.29})_2$, the As and P heights are 1.332 and 1.151 Å from the Fe plane, respectively [38]. We therefore take an effective pnicogen height of 1.28 Å in our calculation, which is the average height of As and P in $BaFe_2(As_{0.71}P_{0.29})_2$ determined experimentally. This effective As/P height (1.28 Å) is less than the As height (1.36 Å) in the $BaFe_2As_2$ but substantially larger than the P height (1.19 Å) in the $BaFe_2P_2$.

In previous inelastic neutron scattering studies of low-energy spin excitations in powder [39] and single crystals [40] of optimally P-doped $BaFe_2(As_{1-x}P_x)_2$, a neutron spin resonance coupled to superconductivity has been identified similar to other iron based superconductors [41–43]. A key conclusion of the work is that the energy of the resonance in $BaFe_2(As_{0.63}P_{0.34})_2$ is dispersive along the c axis, indicating its close connection to the three dimensional AF spin correlations [40]. In hole and electron-doped $BaFe_2As_2$, the wave vector evolution of the low-energy spin excitations and the resonance can be well described by quasiparticle excitations through doping dependent hole and electron Fermi surfaces [27, 44]. Although substituting P for As in $BaFe_2(As_{1-x}P_x)_2$ is expected to be isovalent, angle resolved photoemission spectroscopy (ARPES) experiments reveal changed hole and electron Fermi surfaces from $BaFe_2As_2$ to $BaFe_2(As_{0.7}P_{0.3})_2$ [45]. DFT+DMFT calculations also show that with increasing P-doping, the hole Fermi surface with dominating d_{xy} orbital character shrinks whereas the hole Fermi surfaces with dominating d_{xz} and d_{yz} (d_{z^2} near $k_z = \pi$) orbital characters expand and become more three-dimensional along the k_z direction [Figs. 2(a) and 2(b)]. However, the electron Fermi surfaces do not change significantly. Therefore, the electron-hole Fermi surface nesting condition becomes worse with P-doping. This is consistent with the resulting changes in wave vector dependence of spin excitations [Figs. 2(c) and 2(d)], where the low energy spin excitations become weaker and more diffusive in the momentum space in $BaFe_2(As_{0.7}P_{0.3})_2$. Figure 2(e) and 2(f) shows constant-$\mathbf{Q}$ scans at $\mathbf{Q} = (1, 0, 0)$ and $(1, 0, 1)$,

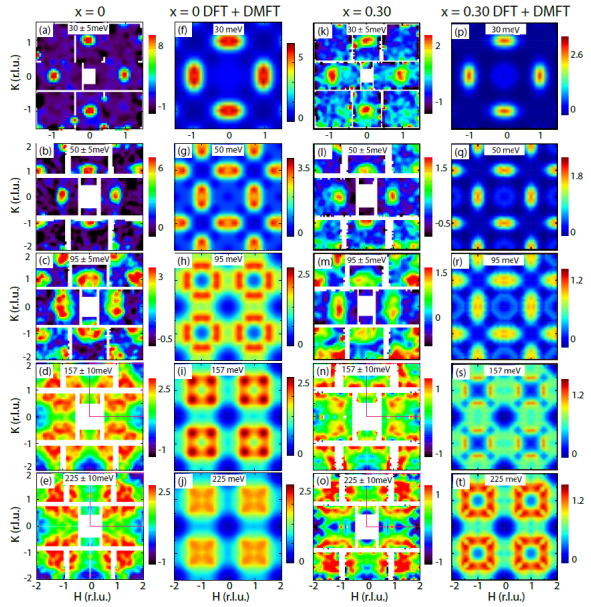

FIG. 3: Wave vector dependence of spin waves of $BaFe_2As_2$ at 7 K and spin excitations of $BaFe_2(As_{0.7}P_{0.3})_2$ at 10 K for energy transfers of (a,k) $E = 30\pm5$ meV [$E_i = 80$ meV and $\mathbf{q} = (H, K, 3)$]; (b,i) $E = 50 \pm 5$ meV [$E_i = 250$ meV and $\mathbf{q} = (H, K, 3)$]; (c,m) $E = 95 \pm 5$ meV [$E_i = 250$ meV and $\mathbf{q} = (H, K, 5)$]; (d,n) $E = 157 \pm 10$ meV [$E_i = 450$ meV and $\mathbf{q} = (H, K, 6)$]; (e,o) $E = 225 \pm 10$ meV [$E_i = 450$ meV and $\mathbf{q} = (H, K, 9)$]. In all cases, the $\pm$ meV indicates the energy integration range. The red boxes in (d,e,n,o) indicate regions that contain nonduplicate data from four fold symmetrizing of the raw data (meaning only the data within the red box is statistically significant, and data in other region of reciprocal space are mirror images of the red box data). (f-j) and (p-t) Calculations of identical energy slices from DFT+DMFT method [46].

respectively, below and above T_c. Consistent with previous work [40], we find that superconductivity-induced resonance is clearly dispersive, occurring at $E_{res} = 12$ meV at $\mathbf{Q} = (1, 0, 0)$ and $E_{res} = 9$ meV at $\mathbf{Q} = (1, 0, 1)$. Figure 2(g) and 2(h) summarizes energy dependence of the low-energy spin excitations at 40 K ($T \approx T_c + 10$ K) and 10 K ($T \approx T_c - 20$ K), respectively. Given the dispersive nature of the resonance, neutron time-of-fight measurements with a fixed incident energy and fixed sample rotation angle in Figs. 2(g) and 2(h) will probe a region of the excitation energies with different L values. Figure 2(i) is temperature differences plot, revealing a clear neutron spin resonance in the energy region of $E \approx 11$ meV and a spin gap below the resonance energy.

Assuming that isovalent P-doping in $BaFe_2(As_{1-x}P_x)_2$ does not change the valence of Fe, the total moment sum rule requires the total magnetic spectral weight M_0, when integrated over all energy and momentum space [$M_0^2 = M^2 + \langle \mathbf{m}^2 \rangle = g^2 S(S+1)$, where M is the static ordered moment, $\langle \mathbf{m}^2 \rangle$ is the local fluctuating moment, $g \approx 2$ is the Landé factor, and S is the spin.], to be independent of P-doping [7]. From Figs. 2(c) and 2(d), we see reduced low-energy spin excitation spectral weight in $BaFe_2(As_{0.7}P_{0.3})_2$ compared with $BaFe_2As_2$, as revealed by the DFT+DMFT calculation [Figs. 1(h) and 4].

Figures 3(a)-3(e) and 3(k)-3(o) compare the two-dimensional constant-energy (E) images of $S(Q, E)$ of spin waves of $BaFe_2As_2$ [30] and spin excitations of $BaFe_2(As_{0.7}P_{0.3})_2$ in the (H, K) scattering plane at different energies. Figures 3(a)-3(e) show the evolution of spin waves of $BaFe_2As_2$ at energy transfers of $E = 30\pm5$, 50 ± 5, 95 ± 5, 157 ± 10, and 225 ± 10 meV, respectively. The corresponding spin excitations of $BaFe_2(As_{0.7}P_{0.3})_2$ are shown in Figs. 3(k)-3(o). At $E = 30 \pm 5$ [Figs. 3(a) and 3(k)] and $E = 50 \pm 5$ meV [Figs. 3(b) and 3(l)], spin excitations in $BaFe_2(As_{0.7}P_{0.3})_2$ form transversely elongated ellipses centered at the in-plane AF zone centers $(\pm1, 0)$ and $(0, \pm1)$ of the undoped $BaFe_2As_2$, but with considerably lower intensity. On increasing the energies to $E = 95 \pm 5$ meV [Fig. 3(m)], spin excitations of $BaFe_2(As_{0.7}P_{0.3})_2$ begin to split transversely from $(\pm1, 0)$, similar to that of spin waves of $BaFe_2As_2$ [Fig. 3(c)]. On further increasing the energy to $E = 157 \pm 10$ [Fig. 3(n)] and $E = 225 \pm 10$ meV [Fig. 3(o)], spin excitations of $BaFe_2(As_{0.7}P_{0.3})_2$ form anisotropic rings centered around $(\pm1, \pm1)$. Figure 1(d) and 1(e) shows spin waves of $BaFe_2As_2$ at $E = 157 \pm 10$ and $E = 225 \pm 10$ meV, respectively. We see that spin waves of $BaFe_2As_2$ at $E = 225\pm10$ meV nearly form a solid spot at $(\pm1, \pm1)$, suggesting that the system has already reached zone boundary at this energy. For comparison, spin excitations of $BaFe_2(As_{0.7}P_{0.3})_2$ at $E = 225 \pm 10$ meV still have a ring structure near $(\pm1, \pm1)$ [Fig. 3(o)], as confirmed by comparison of constant-energy cuts across the data (SFig. 5 in [46]). These results suggest a higher zone boundary energy for $BaFe_2(As_{0.7}P_{0.3})_2$.

To quantitatively compare the experimental results with a combined DFT+DMFT theory [28], we show in Figs. 3(f)-3(j) and 3(p)-3(t) calculated wave vector dependence of spin excitations of $BaFe_2As_2$ and $BaFe_2(As_{0.7}P_{0.3})_2$, respectively, at energies in Fig. 3(a)-3(e) [28]. We see that spin excitations at different energies obtained from the DFT+DMFT calculation in Fig. 3(p)-3(t) have much similarities with the experimental data [Figs. 3(k)-3(o)].

Figure 4(a) and 4(b) shows the calculated dynamical magnetic structure factor $S(Q, E)$ for $BaFe_2As_2$ and $BaFe_2(As_{0.7}P_{0.3})_2$, respectively. Our calculation reveals considerable magnetic spectral weight for energies above 300 meV for both samples contrasting to the vanishing local dynamic susceptibility for energies above 300 meV in $BaFe_2As_2$ [Fig. 1(h)] [47]. The experimentally determined spin excitation dispersion along the $[1, K]$ direction for $BaFe_2(As_{0.7}P_{0.3})_2$ is well captured by the DFT+DMFT calculations [Fig. 4(b)]. For comparison, we also plot in Fig. 4(b) the experimentally determined dispersion along the same direction for $BaFe_2As_2$ as solid

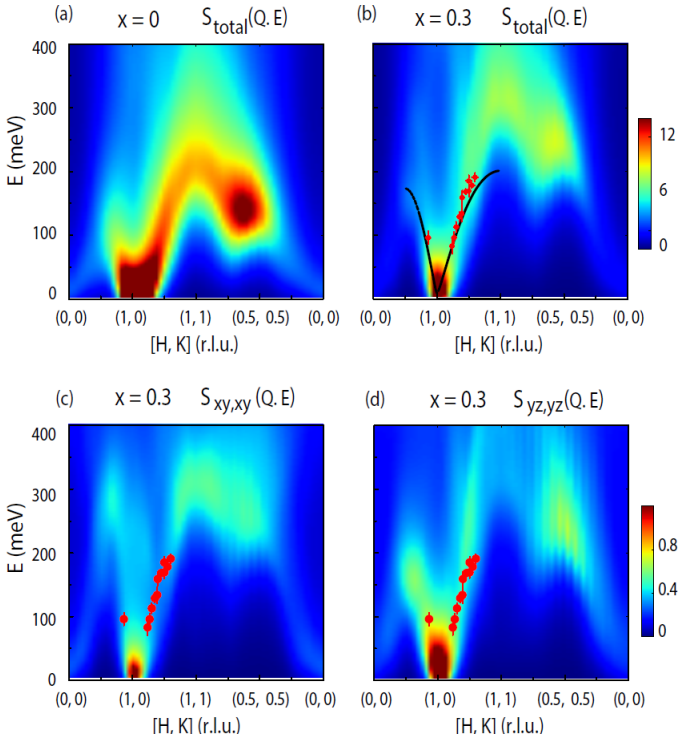

FIG. 4: (a) Calculated total dynamic magnetic structure factor $S(Q, E)$ for (a) $BaFe_2As_2$ and (b) $BaFe_2(As_{0.7}P_{0.3})_2$ using DFT+DMFT. The solid red points in (b) are data from cuts to Fig. 3 and the solid line is the dispersion of $BaFe_2As_2$ from [30]. (c,d) Calculated dynamic magnetic structure factors from the d_{xy}-d_{xy} and d_{yz}-d_{yz} intra-orbital contributions, respectively.

line [30]. To understand different orbital contributions to the spin excitations, we show in Figs. 4(c) and (d) the d_{xy}-d_{xy} and d_{yz}-d_{yz} intra-orbital contribution to the dynamic susceptibility. We see that low-energy spin excitations near $(1, 0)$ are mostly contributed by excitations involving the d_{yz} orbital, while high-energy spin excitations around 300 meV near $(1, 1)$ come mostly from excitations related to d_{xy} orbital. This is in stark contrast with spin excitations in Co-doped LiFeAs compound, where the low-energy spin excitations are dominated by contributions from the d_{xy} orbital [48]. In Ref. [48], it was concluded that the $d_{xz/yz}$ orbitals play an important role in the superconductivity of LiFeAs since their absence in $LiFe_{0.88}Co_{0.12}As$ suppresses superconductivity. The strong low-energy spin excitations contributed by the $d_{yz/xz}$ orbitals in $BaFe_2(As_{0.7}P_{0.3})_2$ shown in Fig. 4(d) suggest that nesting of the $d_{yz/xz}$ orbitals are good for high temperature superconductivity.

Figure 1(h) compares the energy dependence of the local dynamic spin susceptibility for $BaFe_2As_2$, $BaFe_2(As_{0.7}P_{0.3})_2$, and DFT+DMFT calculated values. We see that the peak for local dynamic spin susceptibility for $BaFe_2(As_{0.7}P_{0.3})_2$ occurs around 220 meV, while it is around 180 meV for $BaFe_2As_2$. These results are consistent with energy cuts near the zone boundary for these materials shown in Figs. 1(f) and 1(g). The total fluctuating magnetic moments for $BaFe_2(As_{0.7}P_{0.3})_2$ and $BaFe_2As_2$ are $\langle m^2 \rangle \approx 1.6 \pm 0.2$ (below $\sim$250 meV) and 3.6 μ_B^2 per Fe, respectively [47]. This means that the fluctuating moments of $BaFe_2(As_{0.7}P_{0.3})_2$ are smaller than that of $BaFe_2As_2$ within our energy integration region, consistent with the presence of more magnetic spectral weight at higher energies or a reduced fluctuating moment. These results thus suggest that the decreased iron pnictogen height in iron pnictides from $BaFe_2As_2$ to $BaFe_2(As_{0.7}P_{0.3})_2$ increases the spin excitation bandwidth and decreases the electron correlation effects. Since the reduced pnicogen height due to P doping increases the indirect hopping between Fe $3d$ orbitals and pnicogen p orbitals and weakens the kinetic frustration as the direct hopping between Fe $3d$ orbitals remains almost the same as the Fe-Fe distance changes negligible with P-doping, the band widths of the Fe $3d$ orbitals increase with increasing P doping [46] and the electronic correlation effects decrease. The increased band widths lead to a reduction of the one-particle Green's function, and thus a reduction in the bare two-particle susceptibility. Neglecting the change in the two-particle vertex function due to P doping, this reduction in the bare two-particle susceptibility is responsible for the reduced low energy spin excitation intensity. Similarly, the spin excitation band widths increases due to the reduced pnicogen height in $BaFe_2(As_{0.7}P_{0.3})_2$.

The reduction of the pnicogen height in $BaFe_2(As_{0.7}P_{0.3})_2$ from $BaFe_2As_2$ reduces the low energy spin excitation intensity centered at Q_{AF} and eliminates the static long-range AF order in the undoped $BaFe_2As_2$. At the same time, the pnicogen height in $BaFe_2(As_{0.7}P_{0.3})_2$ is still high enough to maintain intermediate electronic correlation strength with sufficient low-energy spin fluctuations to mediate superconductivity. For spin excitation mediated superconductors [5], superconductivity is controlled by the effective magnetic exchange coupling J and the strength of electron-spin excitation coupling [27]. Since the effective magnetic exchange couplings in $BaFe_2(As_{0.7}P_{0.3})_2$ are considerably larger than those of the $BaFe_2As_2$, it would be interesting to compare superconductivity induced changes in spin excitations of $BaFe_2(As_{0.7}P_{0.3})_2$ and electron/hole-doped $BaFe_2As_2$ [27]. By comparing the absolute intensity changes of the resonance below and above T_c, we find that spin excitations changes across T_c are still much larger than the superconducting condensation energy [46, 49], thus supporting the notion that magnetism is crucial for the superconductivity of $BaFe_2(As_{0.7}P_{0.3})_2$.

In summary, we have used inelastic neutron scattering to map out spin excitations of isovalently doped $BaFe_2(As_{0.7}P_{0.3})_2$. By comparing spin excitations of this material with those of $BaFe_2As_2$ and DFT+DMFT cal-

culations, we conclude that iron pnictogen height in iron pnictides directly controls the spin excitation bandwidth and electron correlations. These results are consistent with the idea that electron correlations in iron-based superconductors arise primarily from the Hund's coupling J_H, and low-energy spin excitations are consequences of nesting between hole and electron Fermi surfaces.

The work at IOP, CAS is supported by NSFC (Projects No. 11374011 and No. 11374346), MOST of China (973 projects: 2012CB821400 and 2015CB921302), and The Strategic Priority Research Program (B) of the Chinese Academy of Sciences (Grant No. XDB07020300). Neutron scattering work at Rice is supported by the U.S. DOE, Office of Basic Energy Sciences, under Contract No. de-sc0012311. Part of the materials work at Rice University is supported by the Robert A. Welch Foundation Grant No. C-1839. The neutron experiment at the Materials and Life Science Experimental Facility of J-PARC was performed under an user program (Proposal No. 2014B0277). The computational work at Rice and Rutgers are supported by NSF DMREF DMR-1436006 and DMR-1435918, respectively.

* Electronic address: yinzhiping@bnu.edu.cn
† Electronic address: pdai@rice.edu

[1] Y. Kamihara, T. Watanabe, M. Hirano, and H. Hosono, J. Am. Chem. Soc. **130**, 3296 (2008).
[2] C. de la Cruz, Q. Huang, J. W. Lynn, J. Li, W. Ratcliff II, J. L. Zarestky, H. A. Mook, G. F. Chen, J. L. Luo, N. L. Wang, and P. C. Dai, Nature **453**, 899 (2008).
[3] S. Jiang, H. Xing, G. Xuan, C. Wang, Z. Ren, C. Feng, J. Dai, Z. Xu, and G. Cao, J. Phys.: Condens. Matter **21**, 382203 (2009).
[4] D. C. Johnston, Adv. Phys. **59**, 803 (2010).
[5] D. J. Scalapino, Rev. Mod. Phys. **84**, 1383 (2012).
[6] T. Shibauchi, A. Carrington, and Y. Matsuda, Annu. Rev. Condens. Matter Phys. **5**, 113 (2014).
[7] P. C. Dai, Rev. Mod. Phys. **87**, 855 (2015).
[8] P. A. Lee, N. Nagaosa, and X.-G. Wen, Rev. Mod. Phys. **78**, 17 (2006).
[9] P. J. Hirschfeld, M. M. Korshunov, I. I. Mazin, Rep. Prog. Phys. **74**, 124508 (2011).
[10] A. Chubukov, Annu. Rev. Condens. Matter Phys. **3**, 57 (2012).
[11] Q. Si and E. Abrahams, Phys. Rev. Lett. **101**, 076401 (2008).
[12] C. Fang, H. Yao, W. F. Tsai, J. P. Hu, and S. A. Kivelson, Phys. Rev. B **77**, 224509 (2008).
[13] C. Xu, M. Muller, and S. Sachdev, Phys. Rev. B **78**, 020501(R) (2008).
[14] D. N. Basov and A. V. Chubukov, Nat. Phys. **7**, 272 (2011).
[15] K. Haule and G. Kotliar, New J. Phys. **11**, 025021 (2009).
[16] Z. P. Yin, K. Haule, and G. Kotliar, Nat. Mater. **10**, 932 (2011).
[17] A. Goerges, L. de' Medici, and J. Mravlje, Annu. Rev. Condens. Matter Phys. **4**, 137 (2013).
[18] C. C. Lee, W. G. Yin, and W. Ku, Phys. Rev. Lett. **103**, 267001 (2009).
[19] F. Krüger, S. Kumar, J. Zaanen, and J. van den Brink, Phys. Rev. B **79**, 054504 (2009).
[20] W. C. Lv, J. S. Wu, and P. Phillips, Phys. Rev. B **80**, 224506 (2009).
[21] C.-C. Chen, J. Maciejko, A. P. Sorini, B. Moritz, R. R. P. Singh, and T. P. Devereaux, Phys. Rev. B **82**, 100504(R) (2010).
[22] B. Valenzuela, E. Bascones, and M. J. Calderón, Phys. Rev. Lett. **105**, 207202 (2010).
[23] G. Kotliar, S. Y. Savrasov, K. Haule, V. S. Oudovenko, O. Parcollet, and C. A. Marianetti, Rev. Mod. Phys. **78**, 865 (2006).
[24] K. Haule, C.-H. Yee, and K. Kim, Phys. Rev. B **81**, 195107 (2010).
[25] M. S. Liu, L. W. Harriger, H. Q. Luo, M. Wang, R. A. Ewings, T. Guidi, H. Park, K. Haule, G. Kotliar, S. M. Hayden, and P. C. Dai, Nat. Phys. **8**, 376 (2012).
[26] H. Park, K. Haule, and G. Kotliar, Phys. Rev. Lett. **107**, 137007 (2011).
[27] M. Wang, C. L. Zhang, X. Y. Lu, G. T. Tan, H. Q. Luo, Y. Song, M. Y. Wang, X. T. Zhang, E. A. Goremychkin, T. G. Perring, T. A. Maier, Z. P. Yin, K. Haule, G. Kotliar, and P. C. Dai, Nat. Commun. **4**, 2874 (2013).
[28] Z. P. Yin, K. Haule, and G. Kotliar, Nat. Phys. **10**, 845 (2014).
[29] S. O. Diallo, V. P. Antropov, T. G. Perring, C. Broholm, J. J. Pulikkotil, N. Ni, S. L. Bud'ko, P. C. Canfield, A. Kreyssig, A. I. Goldman, and R. J. McQueeney, Phys. Rev. Lett. **102**, 187206 (2009).
[30] L. W. Harriger, H. Q. Luo, M. S. Liu, C. Frost, J. P. Hu, M. R. Norman, and P. C. Dai, Phys. Rev. B **84**, 054544 (2011).
[31] R. A. Ewings, T. G. Perring, J. Gillett, S. D. Das, S. E. Sebastian, A. E. Taylor, T. Guidi, and A. T. Boothroyd, Phys. Rev. B **83**, 214519 (2011).
[32] J. T. Park, G. Friemel, T. Loew, V. Hinkov, Yuan Li, B. H. Min, D. L. Sun, A. Ivanov, A. Piovano, C. T. Lin, B. Keimer, Y. S. Kwon, and D. S. Inosov, Phys. Rev. B **86**, 024437 (2012).
[33] H. Q. Luo, X. Y. Lu, R. Zhang, M. Wang, E. A. Goremychkin, D. T. Adroja, S. Danilkin, G. Deng, Z. Yamani, and P. C. Dai, Phys. Rev. B **88**, 144516 (2013).
[34] S. L. Li, C. de la Cruz, Q. Huang, G. F. Chen, T.-L. Xia, J. L. Luo, N. L. Wang, and P. C. Dai, Phys. Rev. B **80**, 020504(R) (2009).
[35] C. L. Zhang, L. W. Harriger, Z. P. Yin, W. C. Lv, M. Y. Wang, G. T. Tan, Y. Song, D. L. Abernathy, W. Tian, T. Egami, K. Haule, G. Kotliar, and P. C. Dai, Phys. Rev. Lett. **112**, 217202 (2014).
[36] D. Hu, X. Y. Lu, W. L. Zhang, H. Q. Luo, S. L. Li, P. P. Wang, G. F. Chen, F. Han, S. R. Banjara, A. Sapkota, A. Kreyssig, A. I. Goldman, Z. Yamani, Ch. Niedermayer, M. Skoulatos, R. Georgii, T. Keller, P. S. Wang, W. Q. Yu, and P. C. Dai, Phys. Rev. Lett. **114**, 157002(2015).
[37] J. M. Allred, K. M. Taddei, D. E. Bugaris, S. Avci, D. Y. Chung, H. Claus, C. de la Cruz, M. G. Kanatzidis, S. Rosenkranz, R. Osborn, and O. Chmaissem, Phys. Rev. B **90**, 104513 (2014).
[38] M. Rotter, C. Hieke, and D. Johrendt, Phys. Rev. B 82, 014513 (2010).
[39] M. Ishikado, Y. Nagai, K. Kodama, R. Kajimoto, M. Nakamura, Y. Inamura, S. Wakimoto, H. Nakamura, M.

Machida, K. Suzuki, H. Usui, K. Kuroki, A. Iyo, H. Eisaki, M. Arai, and S. I. Shamoto, Phys. Rev. B **84**, 144517 (2011).
[40] C. H. Lee, P. Steffens, N. Qureshi, M. Nakajima, K. Kihou, A. Iyo, H. Eisaki, and M. Braden, Phys. Rev. Lett. **111**, 167002 (2013).
[41] M. D. Lumsden, A. D. Christianson, D. Parshall, M. B. Stone, S. E. Nagler, G. J. MacDougall, H. A. Mook, K. Lokshin, T. Egami, D. L. Abernathy, E.A. Goremychkin, R. Osborn, M. A. McGuire, A. S. Sefat, R. Jin, B. C. Sales, and D. Mandrus, Phys. Rev. Lett. **102**, 107005 (2009).
[42] S. Chi, A. Schneidewind, J. Zhao, L.W. Harriger, L. Li, Y. Luo, G. Cao, Z. Xu, M. Loewenhaupt, J. Hu, and P. C. Dai, Phys. Rev. Lett. **102**, 107006 (2009).
[43] D. S. Inosov, J. T. Park, P. Bourges, D. L. Sun, Y. Sidis, A. Schneidewind, K. Hradil, D. Haug, C. T. Lin, B. Keimer, and V. Hinkov, Nat. Phys. **6**, 178 (2010).
[44] H. Q. Luo, Z. Yamani, Y. C. Chen, X. Y. Lu, M. Wang, S. L. Li, T. A. Maier, S. Danilkin, D. T. Adroja, and P. C. Dai, Phys. Rev. B **86**, 024508 (2012).
[45] Y. Zhang, Z. R. Ye, Q. Q. Ge, F. Chen, Juan Jiang, M. Xu, B. P. Xie, and D. L. Feng, Nat. Phys. **8**, 371 (2012).
[46] See supplementary information for more details.
[47] L. W. Harriger, M. S. Liu, H. Q. Luo, R. A. Ewings, C. D. Frost, T. G. Perring, and P. C. Dai, Phys. Rev. B **86**, 140403(R) (2012).
[48] Yu Li, Z. P. Yin, X. C. Wang, D. W. Tam, D. L. Abernathy, A. Podlesnyak, C. L. Zhang, M. Wang, L. Y. Xing, C. Q. Jin, K. Haule, G. Kotliar, T. A. Maier, and P. C. Dai, Phys. Rev. Lett. 116, 247001 (2016).
[49] Z. Diao, D. Campanini, L. Fang, W.-K. Kwok, U. Welp, and A. Rydh, Phys. Rev. B **93**, 014509 (2016).